

ANALYSIS OF MASONRY SHEAR STRENGTH TESTS USING FRACTURE MECHANICS

M. A. Adnan¹ and S.L. Lissel²

Abstract

Shear failure of unreinforced masonry (URM) occurs by brittle fracture. Shear strength of unbonded masonry joints can be determined by using H-shaped test specimens. Failure of these specimens also occurs by a sudden brittle fracture along a mortar-brick interface. Due to the presence of normal tensile stresses, in addition to shear stresses, on the failure plane, crack propagation occurs in a mixed mode (mode *I* and mode *II*). In this paper, finite element analysis is used to determine the rate of energy release as the crack grows in length. The energy release rate is then used to obtain an expression for the stress intensity factor (SIF) associated with the crack. Since the SIF is a function of the applied load and crack length, the critical value of the SIF is estimated by using data obtained from actual tests.

Keywords

shear, fracture, stress intensity, interface

1 Introduction

Masonry in shear or tension can be considered as a quasi-brittle material with little or no plastic deformation before fracture. Under these loads, masonry behaves as a linear elastic material up to the peak load and then fractures (Pluijm, 1999). The softening or descending branch of the stress-strain curve that is often reported in literature is not considered to be an intrinsic part of material behaviour but rather is caused by the characteristics of the testing machine. Similar behaviour is observed in concrete also (Chen, 1982). It is thus reasonable to treat masonry in shear or tension as linear elastic till fracture and apply linear elastic fracture mechanics to it.

H-shaped specimens (Fig. 1) to test for masonry joint shear strength were used at the University of Newcastle, Australia (Lissel et al. 2000.) They have three parts: a “web” and two “flanges” (the terminology is due to the resemblance, in plan, with a steel I beam section.) These test specimens have the advantage of simulating loading

¹ M. A. Adnan, Graduate Student, Dept. of Civil Engg, University of Calgary, Canada.
maadnan@ucalgary.ca

² S. L. Lissel, Assistant Prof., Dept. of Civil Engg, University of Calgary, Canada,
sllissel@ucalgary.ca

conditions at masonry wall joints more realistically as compared to other masonry shear strength test arrangements. In addition, no testing rig is needed to hold the specimen when it is tested because the specimen is stable under test loads. The shearing load applied to the web causes a sudden failure of the joint between one of the flanges and the web, with the failure of the second joint usually occurring later in the test. Both bonded and unbonded joints can be tested using these specimens. In this paper only unreinforced and unbonded joints are considered. The failure of these joints occurs by cracking along the mortar-brick interface.

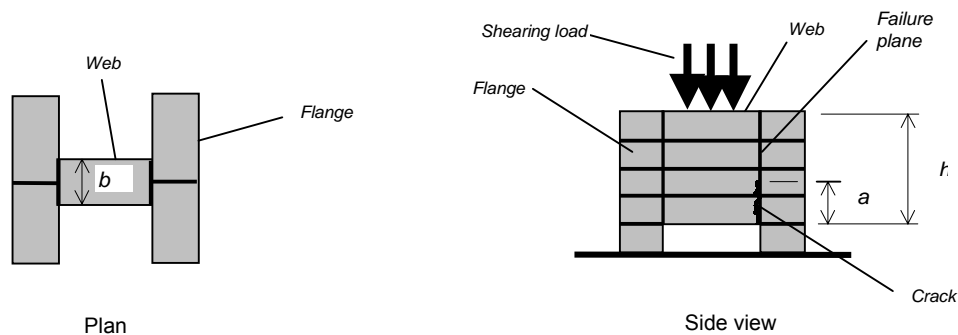


Figure 1: H-shaped masonry test specimen

2 Test Arrangement

The test specimens were built on bases of 600 mm \times 600 mm squares of 20 mm thick plywood. After air curing, the specimen along with the plywood base was placed under a hydraulic loading ram. As mentioned earlier, the test load is applied to the web. To ensure uniform distribution of the load on the upper surface of the web, a rectangle of fibreboard was placed directly over the web. This rectangle had the same dimensions in plan as the web and was 10 mm thick. A 40 mm thick plate of steel was placed between the fibreboard and the ram. A small stabilizing force (1 kN) was applied to each flange.

3 Crack Propagation

It is difficult to trace the propagation of a crack in masonry due to the very fast fracture. Due to the quick propagation of the crack the stiffness of one of the two web-flange joint suddenly decreases. Figs. 2 and 3 show load-deformation curves for specimens made with peach coloured bricks and brown coloured bricks respectively. The deformation used in these figures is the relative displacement between a point on the flange and a point on the web. While they are not based on the displacement of the ram, these figures adequately represent changes in the stiffness of the web-flange joint when cracking occurs. The crack propagated suddenly through the whole depth of the web at the points marked on the curves. Most of the specimens were able to resist higher loads than the first joint fracture load due to interlocking of asperities along the cracked joint and the intact joint between the web and the other flange. The peak load corresponds to the cracking of the other joint after which the specimen broke into three pieces and lost stability. For specimen 2 in Fig. 2 and specimen 3 in Fig. 3, no distinction can be made between the peak load and the first joint fracture load because both joints fractured simultaneously.

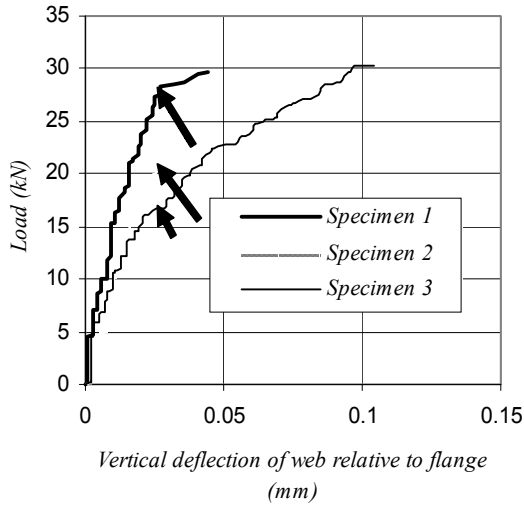


Figure 2: Peach brick curves

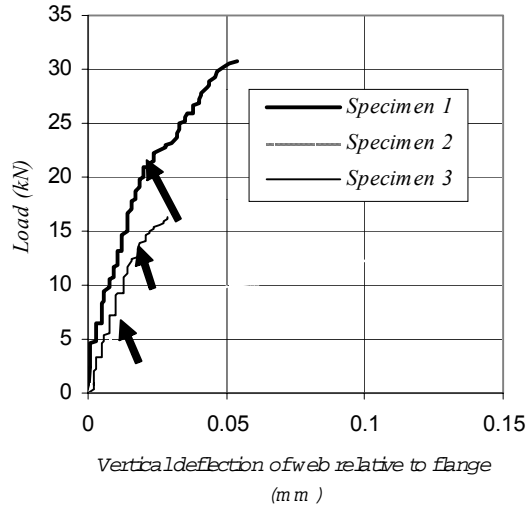


Figure 3: Brown brick curves

4 Relationship between Energy Release Rate and Stress Intensity Factors

The three fundamental modes of crack propagation are opening mode (mode *I*), shearing mode (mode *II*), and tearing mode (mode *III*). Crack propagation can occur in any one of the fundamental modes (*I*, *II*, or *III*) or in a combination of the fundamental modes (*I* + *II* + *III*, *I* + *II*, *I* + *III*, etc). Each mode, *j*, has an associated stress intensity factor, K_j . The crack propagation energy release rate, G , is defined as the energy released per unit increase in crack length per unit width of the crack front. Paris and Sih (1965) showed that there were direct relations between energy release rates and stress intensity factors. The relation between G and the three stress intensity factors (K_I , K_{II} , and K_{III}) for an isotropic material under plane strain conditions is:

$$G = \frac{1-\nu^2}{E} K_I^2 + \frac{1-\nu^2}{E} K_{II}^2 + \frac{1+\nu}{E} K_{III}^2 \quad (1a)$$

Under plane stress conditions the relation is:

$$G = \frac{K_I^2}{E} + \frac{K_{II}^2}{E} + \frac{K_{III}^2}{E} \quad (1b)$$

E and ν are the modulus of elasticity and Poisson's ratio, respectively, of the material through which the crack propagates. These relations are applicable to an isotropic and homogenous material. Masonry is neither isotropic nor homogenous and the crack being considered runs along the mortar-brick interface rather than through the mortar only. For an interface crack between two dissimilar materials which are isotropic and linearly elastic, the following relation given by Malyshev and Salganik (1965) is reproduced with the subscripts modified to suit the current context:

$$G = \frac{1}{16 \cosh^2(\alpha\pi)} \left(\frac{\kappa_m + 1}{\mu_m} + \frac{\kappa_b + 1}{\mu_b} \right) (K_I^2 + K_{II}^2) \quad (1c)$$

where α is a bi-material constant as follows:

$$\alpha = \frac{1}{2\pi} \ln \left(\frac{\mu_m \kappa_b + \mu_b}{\mu_b \kappa_m + \mu_m} \right) \quad (1d)$$

μ_m and μ_b are the shear moduli for mortar and brick respectively. κ_m and κ_b are defined for plane strain as:

$$\begin{aligned}\kappa_m &= 3 - 4\nu_m \\ \kappa_b &= 3 - 4\nu_b\end{aligned}\tag{1e}$$

and for plane stress as:

$$\begin{aligned}\kappa_m &= (3 - \nu_m)/(1 + \nu_m) \\ \kappa_b &= (3 - \nu_b)/(1 + \nu_b)\end{aligned}\tag{1f}$$

ν_m and ν_b are the Poisson's ratios for mortar and brick respectively. A K_{III} term is not included in (1c) but this does not matter as the symmetry of the test arrangements ensures that crack propagation cannot occur in the tearing mode. If both the materials are identical, (1c) reduces to either (1a) or (1b).

5 Computation of G

The value of G could have been obtained directly from the experimental data if it had been possible to measure values of applied load and displacement corresponding to different lengths of the crack. However, due to the fast growth of the crack and limitations of the equipment available this was not possible. Hence, an alternate approach based on the finite element method given in Dixon and Strannigan (1972) will be used in a slightly modified form.

It will be assumed that the loading frame and the body of the hydraulic ram are very stiff as compared to the specimen, the fibreboard, and the plywood base. Thus, the contribution of the loading frame and ram to the storage and release of strain energy can then be conveniently neglected and the fracturing system consists of specimen, particle board and plywood base. The stiffness, S , of the fracturing system for a particular crack length, a , is defined as:

$$S = \frac{P}{D}\tag{2}$$

where P is the load applied by the ram to the fracturing system and D is the displacement of the load for a particular crack length. Stiffness, S , is thus a function of the crack length, a . During the propagation of the crack it is probable that neither P nor D remain constant. However, for simplicity in calculating energy release rates, it is usual to assume that either P or D remains constant when the crack propagates. It can be easily shown that assuming P is constant during crack propagation will give the same results as assuming D is constant during crack propagation (Jayatilaka, 1979). Therefore, it will be assumed that crack propagation occurs at constant load. From (2):

$$D = \frac{P}{S}\tag{3}$$

Since P is assumed to remain constant while the crack propagates and S is a function of a , D is a function of a alone. Differentiating (3) with respect to a :

$$\frac{dD}{da} = -\frac{P}{S^2} \left(\frac{dS}{da} \right)\tag{4}$$

The work done by the load, P , on the fracturing system per unit increase in crack length is:

$$P \left(\frac{dD}{da} \right) = -\frac{P^2}{S^2} \left(\frac{dS}{da} \right)\tag{5}$$

The strain energy stored in the fracturing system is:

$$U = \frac{P^2}{2S} \quad (6)$$

Since P is assumed to remain constant while the crack propagates and S is a function of a , U is also a function of a alone. The change in U per unit increase in crack length is:

$$\frac{dU}{da} = -\frac{P^2}{2S^2} \left(\frac{dS}{da} \right) \quad (7)$$

The energy released during a unit increase in crack length is the work done by the load, P , on the fracturing system during this increase minus the change in strain energy that occurs during this increase. Thus by definition:

$$G = \frac{1}{b} \left[P \left(\frac{dD}{da} \right) - \frac{dU}{da} \right] = -\frac{P^2}{2bS^2} \left(\frac{dS}{da} \right) \quad (8)$$

where b is the width of the web. The energy released is a non-negative quantity since dS/da is either zero or negative. It is convenient to group together all terms that depend on a in one variable and express (8) as:

$$G = \frac{P^2 Z^2}{2b} \quad (9)$$

with

$$Z = \frac{1}{S} \sqrt{-\frac{dS}{da}} \quad (10)$$

6 Finite Element Model

The purpose of the finite element model was not to determine stresses in the specimen or at the crack tip, but to evaluate the stiffness of the fracturing system. Since the stiffness was to be used for determining the rate of energy release, it was essential to include the plywood and the fibreboard components of the test setup in the finite element model. The plywood and fibreboard are relatively soft (compared to the masonry), so the amount of strain energy stored or released from components made out of them cannot be neglected. On the other hand, the loading frame and the hydraulic ram are very stiff and their contribution to strain energy transformations was neglected.

The masonry was assumed to be a homogenous and isotropic material with an average modulus of elasticity of 20,000 MPa. The compressive strength of the masonry was 25 MPa. The use of the smeared value is reasonable because we are interested in only the overall stiffness of the specimen rather than any localized phenomenon. The moduli of elasticity for the plywood and fibreboard were taken as 10,000 MPa and 3,500 MPa respectively.

7 Relationship between Z and a :

Referring to (10), Z depends on the stiffness, S , and the derivative of the stiffness with respect to the crack length, dS/da . Both of these are functions of the crack length, a . Stiffness values obtained by finite element analysis of test specimens with crack lengths of 0 mm, 30 mm, 70 mm, 110 mm, 150 mm, 190 mm, 230 mm and 260 mm were used to plot the stiffness-crack length curve (Fig. 4).

The height of the web, h , is 260 mm. When the crack length reaches this value the joint is completely cracked. However at this stage, the value of S is not zero because the joint between the web and the other flange is still intact. The small force applied to this flange stabilizes the actual specimen. However, separation of one flange changes

the geometry and boundary conditions of the test setup and it is not meaningful to compare the results for $a = h = 260$ mm with those for other values of a . Thus Fig. 4 does not include values for $a = 260$ mm.

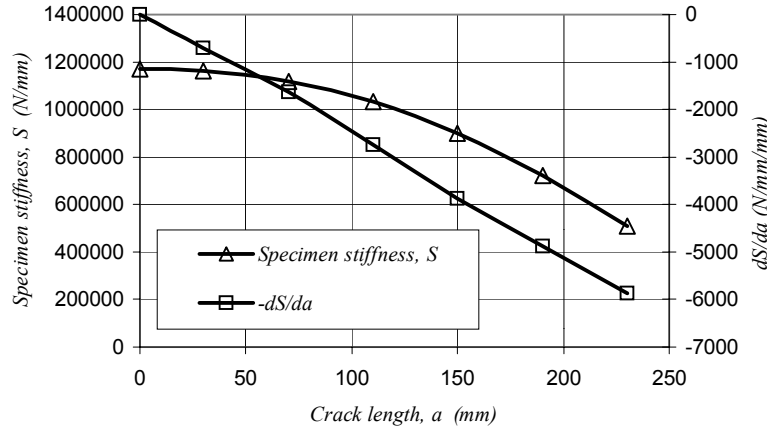


Figure 4: Specimen stiffness S , and dS/da

The value of dS/da for $a = 0$ mm was taken as zero. Values of dS/da for the other crack lengths were obtained from the values of S by the central difference approximation. The value of dS/da corresponding to the final crack length of 230 mm was obtained by extrapolation. From Fig. 4 it is clear that dS/da is a linear function of a :

$$\frac{dS}{da} = -25.66a \quad (11)$$

Integrating (11) and applying the boundary condition that $S = 1,172,000$ N/mm at $a = 0$ mm yields:

$$S = 1172000 - 12.83a^2 \quad (12)$$

Substituting these values in (10) gives

$$Z = \frac{\sqrt{25.66a}}{1172000 - 12.83a^2} \quad (13)$$

8 The Effective Stress Intensity Factor, K_E

“Shearing” failure of the joint seems to be initiated by horizontal tensile stress at the bottom of the joint but the propagation of the crack occurs in a combination of modes *I* and *II*. As mentioned before, mode *III* does not exist due to symmetry of the test setup, thus K_{III} is zero.

On the basis of the values reported by Khalil (1983), ν_m and ν_b can be taken as 0.2 and the modulus of elasticity of mortar, E_m , as 7,000 MPa. The modulus of elasticity of the bricks, E_b , is estimated to be 21,000 MPa. These values of E_m , E_b , ν_m and ν_b lead to $\mu_m = 3,000$ N/mm² and $\mu_b = 9,000$ N/mm², and thus (1c) with (1d) and (1e) gives:

$$K_I^2 + K_{II}^2 = 0.0000858G \quad (14)$$

An interface effective stress intensity factor, K_E , can be defined as:

$$K_E = \sqrt{K_I^2 + K_{II}^2} \quad (15)$$

The mathematical background of K_E is given by Rice and Sih (1965) and Yuuki and Cho (1989). Using (9), (13), (14) and (15) gives:

$$K_E = \left(\frac{0.00926P}{1172000 - 12.83a^2} \right) \left(\sqrt{\frac{25.66a}{2b}} \right) \quad (16)$$

Substituting $b = 90$ mm in (16) gives:

$$K_E = \frac{0.0035P\sqrt{a}}{1172000 - 12.83a^2} \quad (17)$$

9 Application to Test Results

Masonry joints have flaws due to the improper bonding of mortar to bricks and cavities left in the mortar due to poor workmanship. Shrinkage of wet mortar can also cause flaws. These flaws act as starter cracks. If in (17) a is taken as the initial length of a flaw, then the value of P which causes K_E to equal a critical value, K_{EC} , will be the fracture load at which rapid crack propagation occurs. It is assumed that the flaw is at the base of the joint and extends across the full width of the joint. Using an approach similar to that used for concrete where the size of flaws is assumed to be of the same order as the maximum size of the aggregate, the length of the initial flaws in masonry can be taken to be of the same order as the dimensions of a brick (Pant, 1979). In this case the relevant dimension is the height of a brick (≈ 60 mm). The maximum probable flaw size can be assumed to be 10 mm. For a given K_{EC} this will correspond to the lower values of fracture loads, thus from the data in Fig. 2, P can be selected as 15,000 N. Using these values in (17) gives $K_E = K_{EC} = 0.00014 \text{ N/mm}^{1.5}$ ($4.4 \times 10^{-6} \text{ MPa-m}^{0.5}$). The curves with higher fracture loads probably correspond to smaller flaw sizes.

10 Dependence of K_{EC} on Specimen Shape and Size

Yuuki et al. (1994) have shown that for a crack propagating in mixed mode along an aluminium-epoxy interface, K_{EC} depends on the ratio of K_{II} to K_I . It is reasonable to assume that a similar condition exists for mortar-brick interfaces. The ratio of K_{II} to K_I depends on the specimen geometry. Thus, K_{EC} is different from K_{IC} , K_{IIC} and K_{IIIC} , in that it is not a material property.

11 Dependence of K_E on Specimen Shape and Size

The constants in (17) depend on the specimen shape and dimensions. The most important parameter related to specimen shape is the ratio of the horizontal dimension of the web to its vertical dimension. A general form of (17) is obtained from (16) as:

$$K_E = \left(\frac{\gamma P}{S_o - 0.5\beta a^2} \right) \left(\sqrt{\frac{\beta a}{2b}} \right) \quad (18)$$

where S_o and β are functions of specimen shape, size and material properties. S_o is the value of the specimen stiffness, S , for an uncracked specimen. β is the decrease in S per unit increase in crack length per unit crack length. γ can be traced to (1c) and it is a function of only the elastic properties of brick and mortar. It is given by:

$$\gamma = \left[\frac{1}{16 \cosh^2(\alpha\pi)} \left(\frac{\kappa_m + 1}{\mu_m} + \frac{\kappa_b + 1}{\mu_b} \right) \right]^{-0.5} \quad (19)$$

For the specimens tested, S_o is 172000 N/mm, β is 25.66 N/mm³ and γ is 0.00926 N^{0.5}/mm.

12 Conclusions

Finite element analysis was combined with solutions from the theory of elasticity (Equations 1a through 1f) to determine an expression for the effective stress intensity factor. This expression was used with fracture loads from tests to find the critical value, K_{EC} , of this effective stress intensity factor. However, K_{EC} is not a material property; it also depends on the specimen size and shape. To be useful, K_{EC} values have to be associated with specimen size and shape. Specimens with different sizes and shapes have to be actually built and tested. Their fracture loads can be used to determine K_{EC} using a more general form of (18). An equation relating K_{EC} with specimen size and shape can then be obtained. Equations for K_E and K_{EC} can then be used for a fracture mechanics-based approach to the design of unreinforced joints between masonry walls. The more general form of (18) can be developed by using finite element analysis to determine the effect of changing the specimens' parameters (size, shape and material properties) on the quantities S_o and β .

References:

- Chen, W.F. (1982), *Plasticity in Reinforced Concrete*, McGraw-Hill Text, New York, NY.
- Dixon, W.R. and Strannigan, J.S. (1972), Determination of Energy Release Rates and Stress Intensity Factors by the Finite Element Method, *Journal of Strain Analysis*, Vol. 7 No. 2
- Jayatilaka, A.S. (1979), *Fracture of Engineering Brittle Materials*, Applied Science Publishers, London, U.K.
- Khalil, M.R.A. (1983), *Three-dimensional Stress Analysis of Hollow Masonry*, Ph.D. Thesis, University of Calgary, Calgary, Canada.
- Lissel, S. L., Shrive, N. G. and Page, A. W. (2000) Shear in plain, bed joint reinforced, and post-tensioned masonry, *Canadian J. of Civil Engng*, v 27, n 5, 1021-1030
- Malyshev, B.M. and Salganik, R.L. (1965), The Strength of Adhesive Joints using the Theory of Cracks, *International Journal of Fracture*, Vol 1. 114-128
- Pant, B. (1979), Fracture Mechanics in Relation to Failure in Masonry Dams, *Proceeding of an International Conference on Fracture Mechanics in Engineering Application*, Bangalore, India
- Paris, P.C. and Sih, G.C.M. (1965), Stress analysis of cracks, *Symp. Fracture toughness testing and its application*, ASTM Special Technical Publication 381, 30-83.
- Pluijm, R. (1999), *Out-of-Plane Bending of Masonry – Behaviour and Strength*, Ph.D. Thesis, Eindhoven University of Technology, Netherlands
- Rice, J.R. and Sih, G.C. (1965), Plane Problems of Cracks in Dissimilar Media, *Journal of Applied Mechanics*, Vol 32, No. 2, 418-423
- Yuuki, R. and Cho, S. (1989), Efficient Boundary Element Analysis of Stress Intensity Factors for Interface Cracks in Dissimilar Materials, *Engineering Fracture Mechanics*, Vol. 34, No. 1, 179-188
- Yuuki, R., Liu, J., Xu, J., Ohira, T. and Tomoyoshi, O. (1994), Mixed Mode Fracture Criteria for an Interface Crack, *Engineering Fracture Mechanics*, Vol. 47, No. 3, 367-377